2013 IEEE/RSJ International Conference on
Intelligent Robots and Systems (IROS)
November 3-7, 2013. Tokyo, Japan

Design and Sensing of a Flexible Robot Leg

Gabriel A.D. Lopes and Fankai Zhang

Abstract— **This paper reports on the work completed towards the design and sensing of a flexible robotic leg with applications to search and rescue and home robotics. Taking inspiration from the tentacles of cephalopods, we have designed and constructed a segmented leg that is driven by a single motor. The overall deformation of the segmented leg is achieved via tendons. Such a design enables the leg to be modular and mountable in any robotic platform that is driven by wheels or tracks. The deformation of the leg is measured in real-time using a fiber optic sensor that can be used for control purposes. We present experimental results for deformation sensing.**

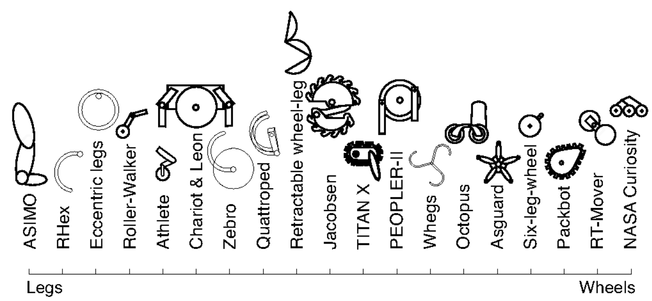

Fig. 1. A spectrum of hybrid locomotion designs ranging from legs to wheels.

I. Introduction

The conditions present during search and rescue scenarios offer more challenges to air, water, and ground locomotion in robotics, than any other environment and situations that can be handled by autonomous robots. Smoke, fire, and confined spaces make flying complex, and debris in the ground or water make walking and swimming difficult. This paper looks at versatile robot "limbs" for locomotion that can be used in search and rescue robots for ground and water scenarios.

The locomotion advantages of legged robots in unstructured and possible unstable terrain, as in the case of search and rescue scenarios, are well established [1]. This is due to the attribute of discrete foot holds with minimal ground interaction present in legged locomotion. In the same way, it is agreed that wheeled solutions are the best suited for flat surfaces. Rolling bodies have very good energetic properties as observed by the cost of transport analysis for various types of wheeled vehicles [2]. For the sake of versatility (agility over rough terrain and power efficiency on flat ground) robots can be endowed with both legs and wheels, but this incurs the cost of an increased number of actuators. Aiming at such versatility, a number of combinations of legs, wheels, and tracks designs have been proposed by the robotics community that can be mapped into a leg-wheel spectrum, as illustrated in Figure 1. Starting on the left side of the spectrum one finds the traditional pure legged robots such as Asimo [3]. The RHex robot [4] uses "half-circle legs" that, although simple, are well adapted to climbing stairs and run efficiently in flat terrain. A variation on the half-circle leg as an off-centered wheel has been presented in [5]. The roller-walker [6] and ATHLETE [7] have legs endowed with wheels at the extremeties. The Chariot robot [8] consists of a body with four legs in the extremities and a pair of wheels in the center of the body. The LEON robot [9] goes beyond the Chariot robot concept by having the pair of wheels reconfigurable into legs, resulting in an hexapod in legged mode. The Quattroped robot [10] follows the same design as RHex in the legged mode: half-circle legs. In the wheeled mode the Quattroped half-circle legs open in the middle resulting in a full circle. After the rotation axis is shifted the leg becomes a full wheel. A retractable wheel-leg design has been proposed in [11] where a circle is divided into three segments that can be used as a 3dof leg. The Jacobsen robot [12] follows a similar design, but in this case the wheel is separated in two by a middle bar, resulting also in a 3dof leg. The Titan X robot [13] is a tracked-legged robot that can morph from a tracked vehicle with four flippers into a quadruped robot. The PEOPLER-II robot [14] has four wheels, each containing two bar elements that can be extended to act as 2dof legs, resulting in the motion of a quadruped. The Whegs robot [15] and ASGUARD [16] follow a different paradigm from most approaches, as their limbs resemble a wheel by assembling various legs in a radial configuration. The Octopus robot [17] combines multiple wheels with rigid links to adapt to various shapes of complex terrain. The "six-leg-wheel" robot [18] consists of six wheels mounted on six swinging legs. The RT-mover [19] has four wheels mounted on rigid links in a sprawled posture. We finish this non-extensive review on the right side of the spectrum: the very successful NASA rover six wheeled design [20]. Although such diversity exist in the robotics ecosystem, in practice in search and rescue applications tracks (combined with "flippers") prevail as the standard of today's deployable robots. This is the case for packbot from iRobot and Quince [21], both utilized in Fukushima disaster site. Tracks with flippers simplify negotiating large obstacles by maximizing the contact of the robot with the ground, albeit at the cost of moderate locomotion speed and relatively high power consumption. By simplifying the

All authors are with the Delft Center for Systems and Control, Delft Robotics Institute, Delft University of Technology, The Netherlands, e-mail: {g.a.delgadolopes, f.zhang}@tudelft.nl

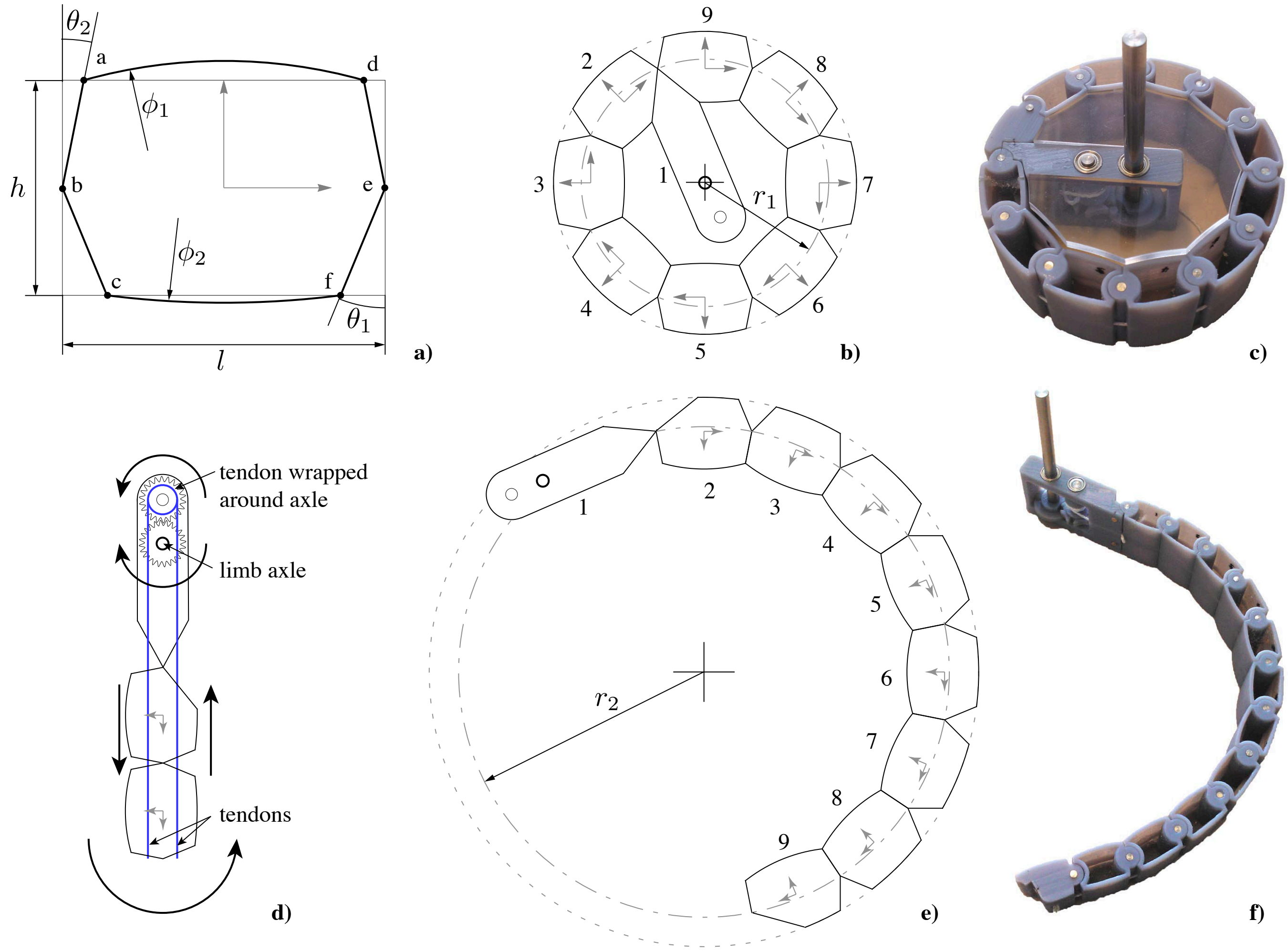

Fig. 2. A segmented leg model. The angles θ_1 and θ_2 in a) dictate the maximum deformation of the leg. In this example the angles are chosen such that in one orientation a wheel configuration is obtained b),c) and a half-circle leg is obtained in the opposite configuration e),f). In d) the internal mechanism of the first leg segment is shown: tendons run inside the full length of the leg and are fixed at the last leg element. The tendons are driven by the limb axle.

locomotion (control design is far less challenging than in the legged case) the research efforts are put on the perception side. We believe that this is a temporary solution for the search and rescue field, and that novel leg-wheel devices should be explored that can keep the number of actuators low and the control design simple, as in the case of the design we propose. The agility of tracked vehicles is nowhere near that of animals like a squirrel or a primate and its power efficiency is less than wheeled vehicles.

The contributions of the paper are as follows: i) in Section II we introduce a new type of deformable leg based on the half-circle design of the RHex robot [4] that can morph from a leg to a wheel and vice versa using a single actuator; ii) in Section III we propose a deformation sensor for this leg based on an optical fiber.

II. Mechanical design

Our aim is to develop a modular and simple mechanical design that allows achieving various leg configurations that can be of use in search and rescue missions. The main criteria chosen for the design are the following:

1) The limb should be driven by a single rotational actuator.

2) It should morph into relevant geometries that can be used for optimal energy consumption, climbing high obstacles, and swim.

3) The geometry of the deformed limb should be actively sensed for control purposes.

4) The limb should be easily mounted in standard wheeled and tracked robotic platforms.

5) The limb should be durable and robust to high impacts.

Following these criteria we have created a segmented leg model presented in Figure 2. In Figure 2.a the base module is illustrated. It consists of a solid element with edge angles and top and bottom curvatures. In these examples we have chosen the parameters such that when assembled with the bottom angled faces touching each other the limb assumes the geometry of a wheel, Figures 2.b and c; and when

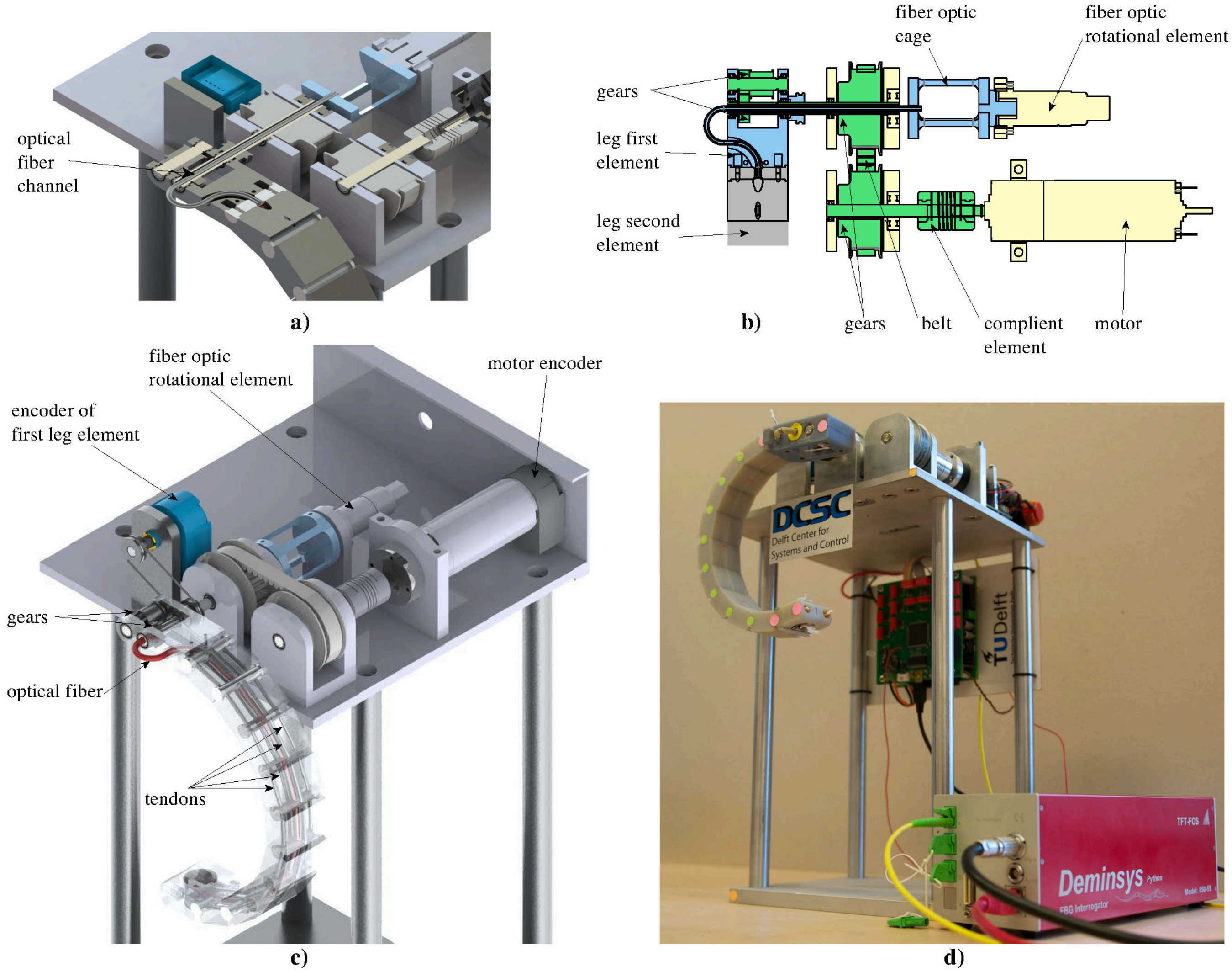

Fig. 3. CAD model and photograph of the prototype flexible leg: a) illustrates a cutout to make visible the channel where the optic fiber is routed to the inside of the leg; b) presents the groups of elements whose motions are directly related: yellow elements are fixed; in blue, the fiber optic cage is rigidly connected to the first element of the leg; in green, the motor shaft drives the large gears and belt to actuate the gears inside the first leg element; c) illustrates a transparent view of the leg where the optical fiber and the tendons are visible; d) is a photograph of the setup, with the interferometer sensor inside the red box. The optical fiber is visible in yellow.

assembled with the top angled faces it becomes a half circle leg, Figures 2.e and f. If the leg is left straight, then it assumes the shape of a fin that can be used for swimming more effectively than the wheel or leg modes. Let the angle γ_i represent the desired arc cover of the leg. In our examples we have that $\gamma_1 = 2\pi$ for a wheel configuration and $\gamma_2 = \pi$ for the half circle configuration. Let n represent the desired number of segments. All the elements in Figure 2.a are calculated using the following simple geometric expressions:

$$\theta_i = \frac{\gamma_i}{2n} \qquad r_i = \frac{l}{2\sin(\theta_i)}$$

$$x_i = \frac{l}{2} - \tan(\theta_i)\frac{h}{2} \qquad \beta_i = \frac{h}{2} + r_i\cos(\theta_i)$$

$$\phi_i = \sqrt{x_i^2 + \beta_i^2}$$

Given these quantities the coordinates of the points in Figure 2.a labeled "a" to "f" are:

$$\begin{array}{lllllll} \text{a} & : & (-x_1, h/2) & \qquad & \text{d} & : & (x_1, h/2) \\ \text{b} & : & (-l/2, 0) & & \text{e} & : & (l/2, 0) \\ \text{c} & : & (-x_2, -h/2) & & \text{f} & : & (x_2, -h/2) \end{array}$$

We have implemented two prototype limbs illustrated in Figures 2.c and 3. For the second, we considered symmetric segments with $\gamma_1 = \gamma_2 = \pi$, i.e. a leg that deforms into half circle legs in both directions. To realize the deformation using a single actuator we have embedded tendons inside the leg segments (see Figure 2.d) that are rigidly attached to the last segment. When the limb axle rotates, a second axel inside the first leg element rotates in the opposite direction. Since the tendons are wrapped around the second axle they deform the leg in the correct direction such that the right orientation for the half circle leg is obtained. The same deformation behavior can be obtained by wrapping the tendons directly into the limb axle and crossing the tendons inside the leg element to change their direction of pulling, avoiding this way the need for second axle. We found, however, this approach to be more complex to implement in practice. The large arrows in Figure 2.d represent the relative motions of the movable elements in the flexible leg. Once the deformation is complete and the tendons are in tension then the entire leg rotates together with the leg axle. The attached video illustrates the functioning of the flexible leg.

The current implementation uses two gears inside the first leg element. This means that the tendons are "back drivable", i.e. by interacting with the leg one can change its geometry. A side effect of this solution is that the leg can change its geometry due to gravity when it is on its top swing position: if the leg falls faster than the rotation of the axle, then the tendons move resulting in a deformation of the geometry. One solution to this problem is by replacing the two gears inside the first element of the leg with a worm gear such that the tendons are not back drivable anymore. In this situation, however, we predict that it is more difficult to achieve a flipper behavior for swimming.

The prototype deformable leg illustrated in Figure 3.d functions as expected, achieving two different configurations when the motor axle is rotated on the right or left orientation. It is however not strong enough to withstand the impacts that the legs of RHex traditionally experience when walking on rough terrain. The critical points of the design are the joints of the leg segments and the play of the tendons. Although we have used Dyneema cable for the tendons (known to be a very stiff cable) the 3D printed leg segments are soft and deform under the high tension of the tendons. This poses some challenges to the construction of robust flexible legs. We believe, however, that through novel monolithic designs where all the components are embedded in a polymer with different levels of compliance, fabricated using shape deposition manufacturing (see e.g. [22]), one can construct robust legs that follow the design proposed here.

III. Leg Deformation Sensing

To measure the deformation of the limb in real-time we have fitted the leg with an optical fiber coated with a fiber Bragg grating (FBG) [23]. The fiber utilized in this prototype has 6 sensors, each with a different grating that reflects the incoming laser at different frequencies. When the fiber is stretched or compressed a shift on the spectral response is visible. Since stretching the fiber results in more reliable readings, the fiber is mounted in the middle of the leg on the top and bottom of a thin flat deformable element. This improves the measurement accuracy of the deformations in both directions. The path of the fiber is the following (see Figure 3.a)): It starts in the optical fiber rotational element (to allow the leg to rotate indefinitely without damaging the fiber), next it goes through the leg shaft. Then, when it reaches the outside of the shaft, the fiber is routed back to the inside of the leg. A curved routing is needed since the fiber has a maximum bending radius of 1 cm. Next, the fiber runs to the end of the leg, circles inside a cavity in the last leg element and returns back to the first leg element. The fiber is terminated inside the first leg element. By creating this "round trip" path inside the leg, deformations in both directions are accurately measured. In effect this results in 3 deformation sensors which are sufficient for qualitative measures of deformation. Note that in our design the fiber is routed on a hollow shaft that is different from the motor shaft. Since there exists motors with hollow shafts, it is possible to route the fiber inside them, simplifying the overall design, at the cost of more specialized motors. Finally, a fiber is connected to the back side of the optical fiber rotational element and to the interferometer sensor (Technobis deminsys), illustrated in Figure 3.d). The interferometer sensor consists of a 256 pixel linear CCD that

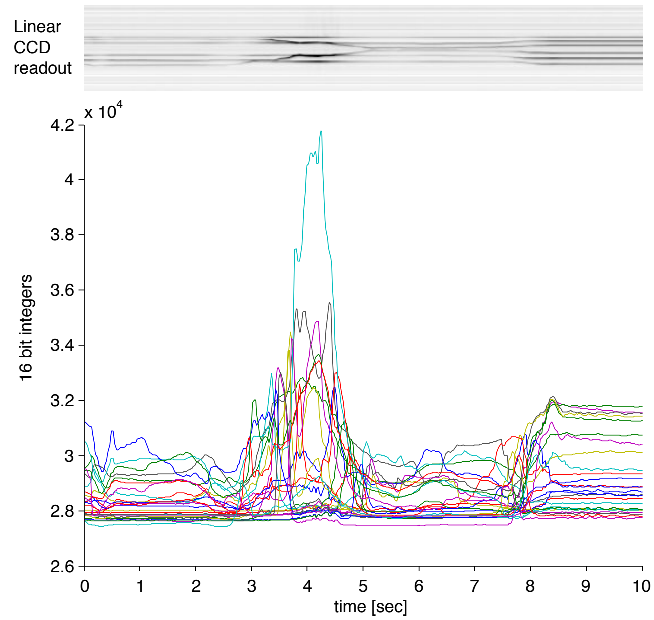

Fig. 4. Input data from the deminsys sensor. The output of the linear CCD is displayed on top in time. The bottom displays the relevant signals that are used for the deformation estimation.

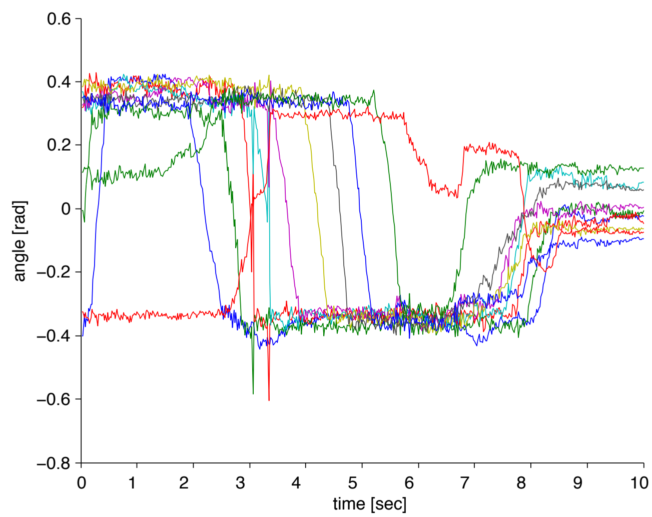

Fig. 5. Unfiltered leg angles measured via ground truth video processing.

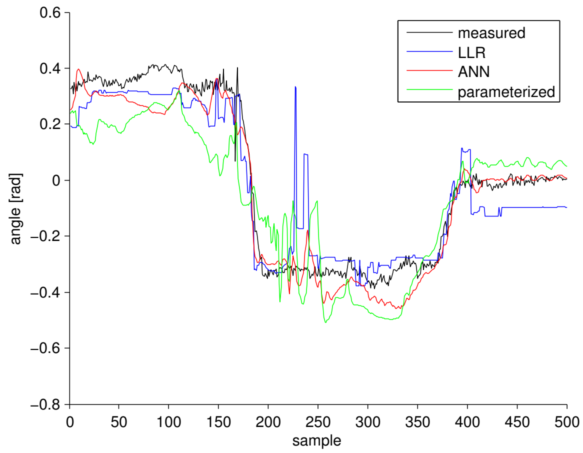

Fig. 6. Estimation results for a single element angle using the validation data as input, plotted against the measured ground truth data obtained via video processing

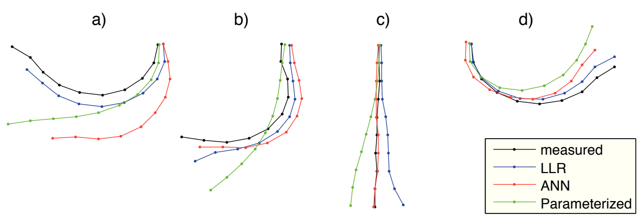

Fig. 7. Fitting results for the validation data using local linear regression, a neural network and a parameterized neural network.

samples the spectrum of the reflected laser at 16 bits per pixel at a rate of up to 20KHz. Figure 4-top illustrates the output of a section of the linear CCD in time when the leg is deformed. This figure shows the spectrum peaks that correspond to the six gratings inside the fiber. When the leg is deformed the peaks shift. The curves presented on the bottom of Figure 4 illustrate the signal readings encoded in 16 bit integers.

In order to predict the deformation of the leg using the CCD information, we ran 8 experiments of 10 seconds each where the leg is manually deformed in various configurations. Markers were added to each segment of the legs and these were tracked using video at 50Hz frame rate (see Figure 3.d)). The CCD sensor was sampled at 500Hz and later resampled to 50Hz to match the video signal. We combined the input from the CCD sensor and the output from the ground truth video (Figure 5) to create a map relating the CCD reading to the geometric deformation. We utilized two supervised learning methods: local linear regression (LLR) [24] and artificial neural networks (ANN).

LLR is a memory-based supervised learning method. During the learning phase samples are simply added to memory. During the prediction phase a collection of nearest neighbors to the queried sample is fitted with an affine function that is used to predict the output of the query sample. For this reason this method is called "lazy" learning in literature [24]. In our system, for each sample measured we store a vector $[X_j^T|Y_j^T]^T$ where $X_j \in \mathbb{R}^{20}$ are 20 pixels from the linear CCD of the interferometer sensor, and $Y_j \in \mathbb{R}^{10}$ are the measured 10 angles of the segmented leg. During normal functioning (after learning) a sample $x \in \mathbb{R}^{20}$ is read from the interferometer sensor. Then, a number k of nearest neighbors $X_{\mathcal{N}} = [X_p \ \dots \ X_{p+k}]$ are extracted from the memory and the predicted leg segment angles $\hat{y}$ are computed using the points $X_{\mathcal{N}}$ and associated learned outputs $Y_{\mathcal{N}} = [Y_p \ \dots \ Y_{p+k}]$ via the expression

$$\hat{y} = Y_{\mathcal{N}} \bar{X}_{\mathcal{N}}^T (\bar{X}_{\mathcal{N}} \bar{X}_{\mathcal{N}}^T)^{-1} x,$$

with $\bar{X}_{\mathcal{N}} = [X_{\mathcal{N}}^T \ \mathbf{1}^T]^T$ and $\mathbf{1}$ a row of ones "1". In our approach we used $k = 20$. We only used 80% of all the samples for learning.

We developed two different ANNs. The first uses as inputs 20 pixels from the linear CCD, and as outputs 10 angles of the segmented leg, with 1 hidden layer. We used the Matlab toolbox to learn the weights of the ANN using 80% of the data for training. The second ANN has 4 outputs that correspond to 4 coefficients of a Fourier expansion that are sufficient to capture the most simple deformation modes: a "C" shape and an "S" shape. We called this the *parameterized ANN*. Figure 6 illustrates the prediction capabilities of the ANN, parameterized ANN, and LLR for the validation data (not used for learning) for a sample of a single leg element. Figure 7 illustrates the predicted leg deformations agains the measure leg geometry for 4 instances. From the results it is clear that the prediction is not perfect but it can be used as a qualitative measure. We obtained the following RMS errors for the data prediction:

Method	RMS	details
LLR	0.311 [rad]	memory with 3200 samples, k=20
ANN	0.302 [rad]	20 inputs, 10 outputs, 1 hidden layer
Parameterized ANN	0.088 [rad]	20 inputs, 4 outputs, 1 hidden layer

Although the parameterized ANN has the lowest RMS for the validation data (predicting each individual segment angle better), in practice the LLR does a better job at matching "geometrically" the curvatures of the deformable leg. We found this result to be counter intuitive, as we expected the opposite. There is room for improvement on the prediction by better training the methods. On the mechanical side, these results can be improved if the grating on the fiber are made with a larger frequency differences or if more gratings are added to the fiber. Although the CCD sensor has 256 pixel, only 20 are utilized in this prototype. Additionally, for high deformations we observed that the spectrum peaks overlaps which can cause ambiguity on the prediction.

IV. Discussion and Conclusions

We have presented a novel tendon-driven deformable leg-wheel driven by a single actuator. Evaluating the desired criteria for the leg design presented in the beginning of Section II we can see that some of the items were achieved:

1) *Limb driven by a single actuator*: we demonstrated that with a single motor different geometries can be achieved. The tendon based design generates the deformation of the leg. Once the range of motion of the tendons is reached the leg is fixed and moves as a whole. The design we present requires a change of the direction of motion in order to switch limb modalities. We acknowledge that this can cause problems is situations where there are tight spaces and it is difficult to turn on the spot to switch from e.g. a wheel to a leg. This hurdle can be solved with more actuation, but violates our original criteria.

2) *Limb deforms into relevant geometries*: our prototype can achieve wheel and leg configurations (Figure 2.c), or half-circle legs on both orientations (Figure 3), and it is able to create a swimming pattern via a flexible fin structure (see attached video media).

3) *Limb deformation sensing*: we have demonstrated deformation sensing in real-time. The solution is at this moment cumbersome due to the large size (and high cost) of the optical fiber rotational element and the interferometer. There are however a number of new developments in industry attempting to reduce the size, weight and power consumption of interferometer sensors. As these developments progress, the current obstacles will fade away. We believe that the embedding of grated fibers in robots with soft and compliant elements can provide an excellent robust and small footprint class of sensors for the future.

4) *Limb easily mountable*: due to the sensing apparatus, it is not easy to mount the leg on a standard platform. If the sensor is removed then this criteria is met.

5) *Limb robust and durable*: the prototype in its current form is not sufficiently strong to be used in actual locomotion. New developments are needed in the mechanical design and choice of materials to achieve durability and robustness.

In this discussion we have left out the control aspect. The prototype leg, due to its tendon operation, requires novel control algorithms that can use the leg deformation sensor in their advantage. If no leg sensing is used, then calibration/observer design become an important element to consider. We are currently developing controllers in simulation for both cases.

V. ACKNOWLEDGMENTS

We thank Laura Bongaardt for the help with the 1st figure and Will van Geest, Ron van Puffelen, and Kees Slinkman for their contributions to the design and implementation of the flexible leg prototype.

REFERENCES

[1] F. Hardarson, "Locomotion for difficult terrain," Dept. Mach. Des., Royal Inst. Technol., Stockholm, Sweden, TRITA-MMK, Tech. Rep., 1998.

[2] J. Yong, R. Smith, L. Hatano, and S. Hillmansen, "What price speed-revisited," *Ingenia*, vol. 22, pp. 46–51, 2005.

[3] M. Hirose and K. Ogawa, "Honda humanoid robots development," *Philosophical Transactions of the Royal Society A: Mathematical, Physical and Engineering Sciences*, vol. 365, no. 1850, pp. 11–19, 2007.

[4] U. Saranli, M. Buehler, and D. E. Koditschek, "RHex: A simple and highly mobile hexapod robot," *The Int. Journal of Robotics Research*, vol. 20, pp. 616–630, 2001.

[5] X. Tan, Y. Wang, and X. He, "The gait of a hexapod robot and its obstacle-surmounting capability," in *Proc. of World Congress on Intelligent Control and Automation*, 2011, pp. 303–308.

[6] S. Hirose and H. Takeuchi, "Study on Roller-Walk (basic characteristics and its control)," in *Proc. of IEEE Int. Conf. on Robotics and Automation*, vol. 4, 1996, pp. 3265–3270.

[7] J. Townsend, J. Biesiadecki, and C. Collins, "ATHLETE mobility performance with active terrain compliance," in *Proc. of IEEE Aerospace Conf.*, 2010, pp. 1–7.

[8] S. Nakajima, E. Nakano, and T. Takahashi, "Motion control technique for practical use of a leg-wheel robot on unknown outdoor rough terrains," in *Proc. of IEEE/RSJ Int. Conf. on Intelligent Robots and Systems*, vol. 2, 2004, pp. 1353–1358.

[9] E. Rohmer, M. Collins, G. Reina, and K. Yoshida, "A novel teleoperated hybrid wheel-limbed hexapod for the exploration of lunar challenging terrains," in *26th Int. Symposium on Space Technology and Science 2008*, 2008, pp. 3902–3907.

[10] K. J. Huang, S.-C. Chen, Y. C. Chou, S.-Y. Shen, C.-H. Li, and P.-C. Lin, "Experimental validation of a leg-wheel hybrid mobile robot quattroped," in *Proc. of IEEE Int. Conf. on Robotics and Automation*, 2011, pp. 2976–2977.

[11] K. Tadakuma, R. Tadakuma, A. Maruyama, E. Rohmer, K. Nagatani, K. Yoshida, A. Ming, M. Shimojo, M. Higashimori, and M. Kaneko, "Mechanical design of the wheel-leg hybrid mobile robot to realize a large wheel diameter," in *Proc. of IEEE Int. Conf. on Intelligent Robots and Systems*, 2010, pp. 3358–3365.

[12] S. Jacobsen, F. M. Smith, M. Olivier, and C. S. Maggio, "Reconfigurable articulated leg and wheel," US Patent US 7 017 687, 03 28, 2006.

[13] R. Hodoshima, Y. Fukumura, H. Amano, and S. Hirose, "Development of track-changeable quadruped walking robot TITAN X-design of leg driving mechanism and basic experiment," in *Proc. of IEEE Int. Conf. on Intelligent Robots and Systems*, 2010, pp. 3340–3345.

[14] T. Okada, W. T. Botelho, and T. Shimizu, "Motion analysis with experimental verification of the hybrid robot PEOPLER-II for reversible switch between walk and roll on demand," *The Int. Journal of Robotics Research*, vol. 29, no. 9, pp. 1199–1221, 2009.

[15] R. Schroer, M. Boggess, R. Bachmann, R. Quinn, and R. Ritzmann, "Comparing cockroach and whegs robot body motions," in *Proc. of IEEE Int. Conf. on Robotics and Automation*, vol. 4, 2004, pp. 3288–3293.

[16] M. Eich, F. Grimminger, and F. Kirchner, "A versatile stair-climbing robot for search and rescue applications," in *Proc. of IEEE Int. Workshop on Safety, Security and Rescue Robotics*, 2008, pp. 35–40.

[17] M. Lauria, Y. Piguet, and R. Siegwart, "Octopus - an autonomous wheeled climbing robot," in *In Proc. of the Fifth Int. Conf. on Climbing and Walking Robots*, 2002.

[18] Y. Li, "Dynamic simulation analyses of a six-leg-wheel hybrid mobile robot under uneven terrains," in *Proc. of Third Int. Conf. on Intelligent Networks and Intelligent Systems*, 2010, pp. 308–311.

[19] S. Nakajima, "RT-Mover: a rough terrain mobile robot with a simple leg-wheel hybrid mechanism," *The Int. Journal of Robotics Research*, pp. 1609–1626, 2011.

[20] E. Tunstel, M. Maimone, A. Trebi-Ollennu, J. Yen, R. Petras, and R. Willson, "Mars exploration rover mobility and robotic arm operational performance," in *IEEE Int. Conf. on Systems, Man and Cybernetics*, vol. 2, 2005, pp. 1807–1814.

[21] K. Nagatani, S. Kiribayashi, Y. Okada, S. Tadokoro, T. Nishimura, T. Yoshida, E. Koyanagi, and Y. Hada, "Redesign of rescue mobile robot quince," in *Proc. of IEEE Int. Symposium of Safety, Security, and Rescue Robotics*, 2011, pp. 13–18.

[22] S. A. Bailey, J. G. Cham, M. R. Cutkosky, and R. J. Full, "Biomimetic robotic mechanisms via shape deposition manufacturing," in *Int. Symposium on Robotics Research*, vol. 9, 2000, pp. 403–410.

[23] K. Hill, Y. Fujii, D. Johnson, and B. Kawasaki, "Photosensitivity in optical fiber waveguides: Application to reflection filter fabrication," *Applied Physics Letters*, vol. 32, no. 10, pp. 647–649, 1978.

[24] T. M. Dietrich Wetterschereck, David Aha, "A review and empirical evaluation of feature weighting methods for a class of lazy learning algorithms," *Artificial Intelligence Review*, vol. 11, pp. 273 – 314, 1997.